J Biol Inorg Chem (2017) 22:739–749
DOI 10.1007/s00775-017-1451-6

MINIREVIEW

Siderophores and mussel foot proteins: the role of catechol, cations, and metal coordination in surface adhesion

Greg P. Maier[1] · **Alison Butler**[1]

Received: 20 February 2017 / Accepted: 22 March 2017 / Published online: 31 March 2017

Abstract Metal coordination, hydrogen bonding, redox reactions, and covalent crosslinking are seemingly disparate chemical and physicochemical processes that are all accomplished in natural materials by the catechol functional group. This review focuses on the reactivity of catechols in *tris*-2,3-dihydroxybenzoyl-containing microbial siderophores and synthetic analogs, as well as Dopa-(3,4-dihydroxyphenylalanine)-containing mussel foot proteins that adhere to surfaces in aqueous conditions. Mussel foot proteins with a high content of Dopa and cationic amino acids, Lys and Arg, adhere strongly to mica, an aluminosilicate mineral, in aqueous conditions. The siderophore cyclic trichrysobactin, *tris*-(2,3-dihydroxybenzoyl-D-Lys-L-Ser) and related synthetic analogs in which the tri-Ser macrolactone is replaced by Tren, *tris*-(2-aminoethyl)amine, also adheres strongly to mica. Variation in the nature of the catechol and cationic groups in synthetic analogs reveals a synergism between the cationic amino acid and the catechol, required for strong aqueous adhesion. Autoxidation and iron(III)-catalyzed oxidation of 2,3-dihydroxy and 3,4-dihydroxy catechols are also considered. These siderophore analogs provide a platform to understand catechol interactions and reactivity on surfaces, which may ultimately improve the design of synthetic materials that address diverse challenges in medicine, materials science, as well as other disciplines, in which surface adhesion in aqueous conditions is important.

✉ Alison Butler
butler@chem.ucsb.edu

[1] Department of Chemistry and Biochemistry, University of California, Santa Barbara, CA 93106-9510, USA

Keywords Catechol · Siderophore · Dopa · Mussel foot protein · Adhesion

Introduction and scope

Catechols are biologically active functional groups found in animals, plants, and microbes (Fig. 1). In its simplest form, the catechol 1,2-dihydroxybenzene is present in some organisms, although derivatized forms of 1,2-dihydroxybenzene form the basis of most biologically significant catechol compounds. The distinguishing side chain of the amino acid L-Dopa is 3,4-dihydroxy-L-phenylalanine (Fig. 1), formed in proteins by the posttranslational hydroxylation of tyrosine. The most common catechol in microbial siderophores, which are compounds produced by bacteria to facilitate sequestration and uptake of Fe(III), is 2,3-dihydroxybenzoic acid (2,3-DHBA; Fig. 1). This catechol is derived from chorismate, which originates via the shikimic acid pathway. Enterobactin, produced by many enteric bacteria, including *E. coli*, is one of the most well-known 2,3-DHBA containing siderophores (Fig. 2), although 3,4-DHBA has been identified in some siderophores, such as petrobactin from *Marinobacter hydrocarbonoclasticus* [1] and *Bacillus anthracis* [2].

Catechols are also present as catecholamines in neurotransmitters, including dopamine, epinephrine, and norepinephrine, as well as in polymerized forms of dopamine, such as the skin pigment melanin (Fig. 1). Other well-known catechols include catechins, members of the flavin-3-ol-class of plant secondary metabolites, isolated from a variety of plants including tea, as well as urushiol, a long-chain alkyl catechol, which is the skin-irritating agent in the poison ivy plant. Humboldt squid beaks contain extensive histidyl–Dopa crosslinks that are formed

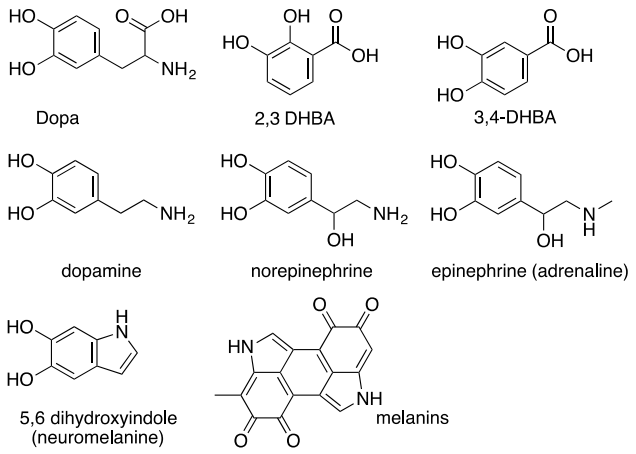

Fig. 1 Structures of biologically derived catechols

as a result of Dopa oxidation [3]. The sandcastle worm *Phragmatopoma californica* secretes a protein-based cement to construct tunnels with exogenous mineral particles [4]. Catechol oxidation within the cement initiates the formation of 5-*S*-cysteinyl-Dopa crosslinks, facilitating the curing process [4].

Catechol is simultaneously a weak acid and a readily oxidized reducing agent. Thus, it is susceptible to one- and two-electron oxidation to semiquinone and to ortho-quinone, respectively. As a 1,2-diol of benzene, catechols coordinate transition metal ions with high affinity, and also undergo metal-catalyzed oxidation and or crosslinking reactions. The focus of this review is the chemistry of 2,3-DHBA and Dopa catechols in the context of adhesion to surfaces in wet aqueous conditions. In this regard, the reactivity of microbial catechol siderophores, mussel foot proteins, and certain synthetic analogs will be covered, including relevant Fe(III) coordination and oxidation chemistry.

Iron coordination by biological catechols

Catechol siderophores

Enterobactin, salmochelin, cyclic trichrysobactin, and bacillibactin are all tris-catecholate siderophores with a tri-ester macrolactone core (Fig. 2). Enterobactin—a natural product of enteric and pathogenic bacteria such as *E. coli*—is the cyclic trimer of 2,3-dihydroxybenzoyl-L-serine (Fig. 2) [5]. Salmochelin, isolated from *Salmonella enterica* and uropathogenic *E. Coli*, retains the structure of enterobactin although with the addition of glucose at the C-5 position on up to two of the catechol rings [6]. Cyclic trichrysobactin derived from the plant pathogen *Dickeya chrysanthemi* contains the triserine lactone scaffold of enterobactin although with a D-Lys spacer inserted between L-Ser and 2,3-DHBA [7]. Bacillibactin, produced by *Bacillus subtilis* and other *Bacilli* species, is based on the lactone of tris-L-threonine with elongated catechol-terminated arms containing a glycine spacer (Fig. 2) [8]. These are just a few examples of the tris-catechol siderophores based on a tris-L-Ser or L-Thr macrolactone scaffold.

Tris-catecholate siderophores coordinate iron(III) with particularly high affinity [9, 10]. The proton-independent stability constants for Fe(enterobactin)$^{3-}$ and Fe(bacillibactin)$^{3-}$ are 10^{49} [11] and $10^{47.6}$ [8], respectively. High-resolution X-ray crystal structures for these siderophore complexes are surprisingly rare. The only X-ray crystal structure of a discrete metal-enterobactin complex is of vanadium(IV)-enterobactin, [V(enterobactin)]$^{2-}$, which reveals a Δ-configuration at the metal center, and lacks a characteristic V(IV) oxo group [12, 13]. The circular dichroism spectrum of [Fe(III)(enterobactin)]$^{3-}$ is also consistent with the Δ-configuration [13], as is the Fe(III) complex of linear enterobactin [14]. Interestingly, the presence of a glycine spacer and a tris-L-Thr lactone core in

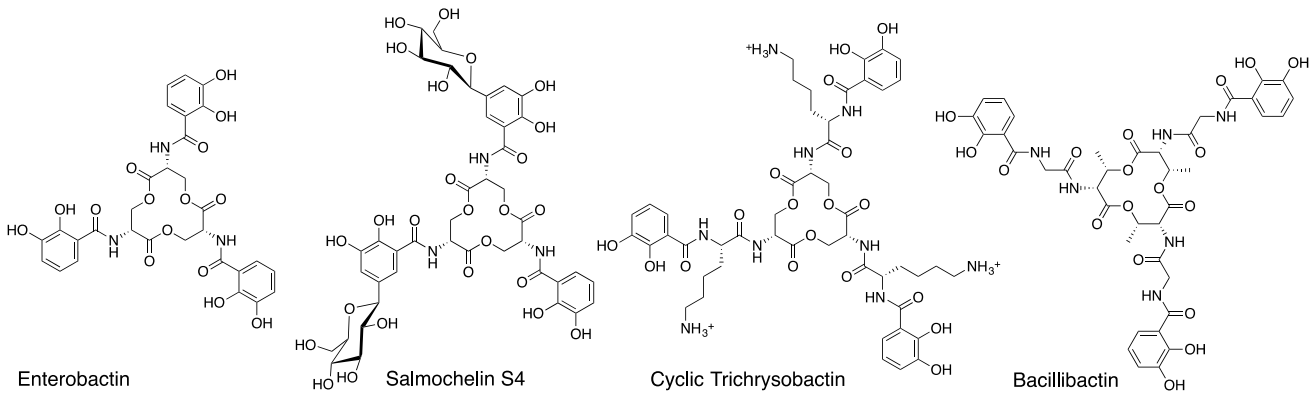

Fig. 2 Structures of enterobactin, salmochelin S4, cyclic trichrysobactin, and bacillibactin

bacillibactin [15] promotes the Λ-configuration [16]. The Fe(III) complexes of cyclic trichrysobactin with a D-Lys spacer and tri-vanchrobactin with a D-Arg spacer have the Λ-configuration, as well [7, 17].

Under physiological conditions, enterobactin coordinates Fe(III) with the three bidentate catecholate groups [18, 19]. At lower pH, however, tris catecholate coordination shifts to tris salicylate coordination, which is induced by protonation of the meta catechol hydroxyl groups. Thus, in the salicylate binding mode, Fe(III) is coordinated by the amide oxygen and the ortho hydroxyl oxygen of 2,3-DHBA [20, 21].

The ester linkages in enterobactin, salmochelin, cyclic-trichrysobactin, and bacillibactin are quite susceptible to hydrolysis, producing the linear tris catechol form, the dimer fragment (e.g., bis-(2,3-dihydroxybenzoyl-L-Ser) for enterobactin), and the monomers (e.g., 2,3-DHBA-L-Ser of enterobactin, 2,3-DHBA-D-Lys-L-Ser of trichrysobactin, etc.). Chrysobactin, 2,3-DHBA-D-Lys-L-Ser [22, 23], and vanchrobactin, 2,3-DHBA-D-Arg-L-Ser [24, 25] were originally reported as monocatechol siderophores. The pKas for the first catechol hydroxyl of chrysobactin and vanchrobactin are substantially lower than that of catechol due to an intramolecular hydrogen bond between the deprotonated ortho hydroxyl and the proton on the adjacent amide nitrogen [25] (Table 1). The logβ_3 stability constants for Fe(III) complexes of chrysobactin, vanchrobactin, catechol, and *N*,*N*-dimethyl-2,3-dihydroxybenzamide are surprisingly not exactly parallel to either the 1st or 2nd pKa of the substituted catechols (Table 1) [25].

Catechol in chrysobactin (i.e., 2,3-DHBA-D-Lys-L-Ser) has been shown to coordinate Fe(III) as mono, bis, and tris complexes, depending on pH (Fig. 3). The pH dependence of binding stoichiometry of chrysobactin in fourfold excess over Fe(III) reveals that tris catecholate coordination dominates at pH >6.1, bis catecholate coordination at pH 6.1 > pH > 4.4, and mono catecholate coordination at pH <4.4 (Fig. 3b).

While 2,3-DHBA is the predominant type of catechol in siderophores, variation in the nature of the catechol does affect Fe(III)-catechol speciation, such as for Dopa, a 3,4-dihydroxy catechol. In a Dopa-functionalized polyethylene glycol (PEG) polymer, tris catecholate coordination dominates at pH >9.1 (with Dopa in threefold excess over $FeCl_3$), bis at 9.1 > pH > 5.6, and mono at pH <5.6 (Fig. 4) [26, 27]. Thus tris-catechol Fe(III) complexation is favored for 2,3-DHBA-type catechols at a lower pH than the 3,4-dihydroxy catechol in Dopa. Nitration of Dopa further impacts the binding stoichiometry. 4-Nitro-Dopa in the functionalized polyethylene glycol (PEG) polymer forms hydrogels at pH 9 which contain largely tris-coordinate crosslinks, whereas the non-nitrated Dopa derivative is predominantly bis-coordinate [28].

Table 1 pKa values and logβ_3 stability constants of selected catechol compounds

Catechol	COOH pKa	1st catechol pKa	2nd catechol pKa	Amine pKa	logβ_3	References
Chrysobactin	3.17	6.73	10.61	12.1	40.2	[23]
Vanchrobactin	3.2	6.79	11.8	13.6	42.7	[24]
Catechol	–	9.32	13.05	–	44.6	[24]
N,*N*-Dimethyl-2,3-dihydroxybenzamide	–	8.42	12.1	–	40.24	[10]

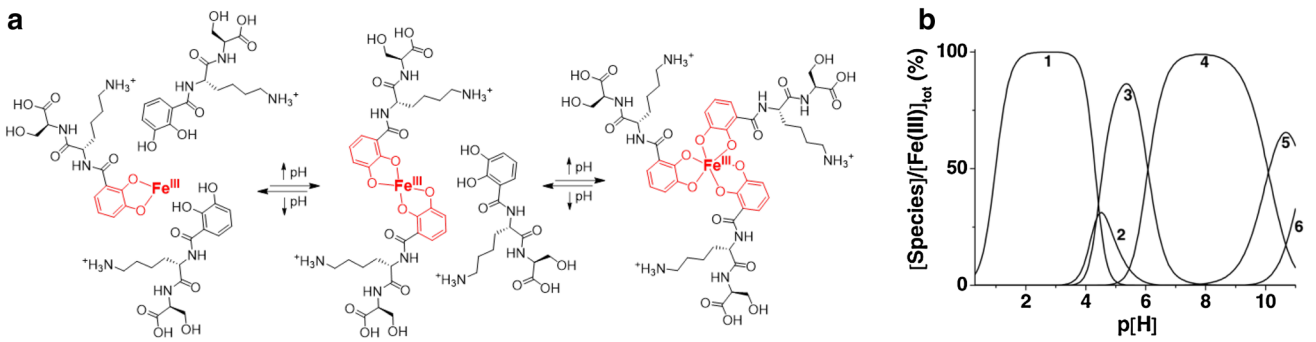

Fig. 3 pH Dependence of Fe(III) coordination by the catechol in chrysobactin. **a** Mono-catechol complexation is favored at low pH and tris-catechol complexation favored at high pH. **b** Distribution diagram of Fe(III)-chrysobactin (*1*) Fe(III)-chrysobactinH_2^{2+}; (*2*) Fe(III)-chrysobactin$_2H_3$; (*3*) Fe(III)-chrysobactin$_2H_2^-$; (*4*) Fe(III)-chrysobactin$_3H_3^{3-}$; (*5*) Fe(III)-chrysobactin$_3H_2^{4-}$; (*6*) Fe(III)-chrysobactin$_3H^{5-}$. Conditions: 4 mM chrysobactin; 1.0 mM $Fe(ClO_4)_3$; $I = 0.1$ M ($NaClO_4$); 25 °C. Figure 3b reproduced from [23]

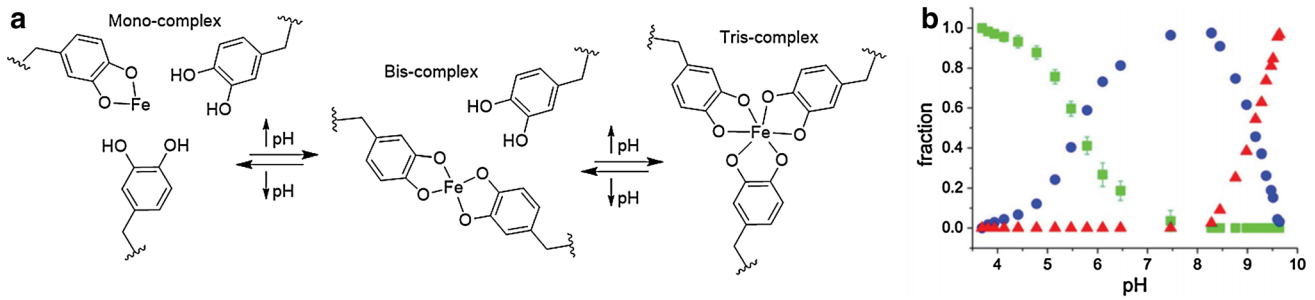

Fig. 4 Fe(III) Coordination to DOPA. **a** Fe(III)-DOPA coordination is pH-dependent, with mono-complexation favored at low pH and tris-complexation favored at high pH. **b** Dopa-modified polyethylene glycol (PEG-Dopa$_4$, 10 kDa PEG core) in solution with $FeCl_3$ (Dopa:Fe(III) ratio = 3:1) shows a pH dependence in the relative fraction of mono- (*green*), bis- (*blue*), and tris-catechol-Fe(III) (*red*) complexes. Figure 4 adapted from [26]

Dopa in marine mussel foot proteins

Mussels adhere to rocks in the intertidal zone through a radial array of adhesive plaques that are tethered to the body of the mussel by protein-rich threads. The adhesive plaques and threads comprise what is known as the byssus. The plaques contain many different mussel foot proteins (Mfps; Fig. 5b). Dopa is found in unusual abundance in many of these Mfps. Mfp-3 and Mfp-5 contain the highest mol% Dopa at 20 and 30 mol%, respectively [29]. Mfp-5 also has 19.5 mol% Lys and 3.1 mol% Arg and HydroxyArg residues, while Mfp-3 has 15.0 mol% Lys and 9.5 mol% Arg and HydroxyArg [30]. Dopa contributes to adhesive plaque performance through interfacial surface priming interactions in the case of Mfp-3 and Mfp-5—described further, below—and through metal coordination, as seen in Mfp-1 and Mfp-2 [31–34].

Raman microscopy shows Dopa coordination to Fe(III) throughout the plaque with a predominance occurring in the outer cuticle and less near the interface between the plaque and the substrate [35]. Mfp-1 is a coating protein that forms the cuticle of the byssal plaque and thread (Fig. 5b) [34, 36, 37]. Two variants of Mfp-1 exist and differ based on the exent of posttranslational hydroxylation of tyrosine to Dopa [33]. The Mfp-1 variant with higher Dopa content is found as hard granules with a high density of Fe(III)–Dopa coordination, as confirmed by Raman microscopy [33]. The Mfp-1 variant with relatively less Dopa forms the protein matrix that surrounds the granules and has a lower density of Fe(III)–Dopa coordination [33]. The high Fe(III)–Dopa crosslink density of the granules imparts hardness, while the low Fe(III)–Dopa crosslink density of the surrounding protein matrix allows for extensibility [33]. Additionally, these hard Fe(III)–Dopa crosslinked granules enable high cuticle failure strains by hindering crack propagation [33]. When the cuticle is strained, microcracks form preferentially within the softer surrounding protein matrix and these cracks extend until obstructed by a harder, more highly crosslinked granule [33, 34, 36]. The importance of Fe(III) to the mechanical properties of the cuticle has been confirmed through EDTA treatment. Raman spectra of EDTA-treated cuticles show significant reduction in Fe(III)–Dopa resonance peaks and the hardness of the EDTA-treated cuticles is reduced by 50% [34]. Reintroduction of Fe(III) to the cuticle is accompanied by recovery of Fe(III)-Dopa resonance peaks in the Raman spectra and highlights the reversible nature of Fe(III)-Dopa crosslinking [34, 38, 39].

Mfp-2, located within the central bulk of the plaque (Fig. 5b), is the most abundant Mfp and contains only 5 mol% Dopa [35]. Mfp-2 is an important structural component of the plaque and, therefore, must interact strongly with itself to ensure strong cohesion within the bulk of the plaque. Fe(III) addition induces strong crosslinking within Mfp-2 [35]. Additionally, mixtures of purified Mfp-2 and Fe(III) precipitated at pH 8 show a resonance Raman signal characteristic of tris Dopa coordination to Fe(III) [35]. The prevalence of Fe(III)–Dopa complexation within Mfp-1 and Mfp-2 contribute to the structural integrity of the adhesive plaques and enable their unique mechanical properties. Dopa in other Mfps (considered below) is utilized for interfacial interactions.

Surface interactions of catechol

Mica—a hydrophilic, negatively charged aluminosilicate mineral—is representative of rocks found in the marine environment. Water and hydrated cations form a tightly bound hydration layer on mica [41]. This hydration layer obstructs the interaction between an adhesive material and the underlying surface which is required for sturdy wet adhesion. Wet adhesive proteins such as surface priming Mfp-3 and 5 are capable of displacing this hydration layer, enabling strong adhesive interactions underwater.

The surface forces apparatus (SFA) is ideally suited to investigations of adhesive materials on a mica surface in

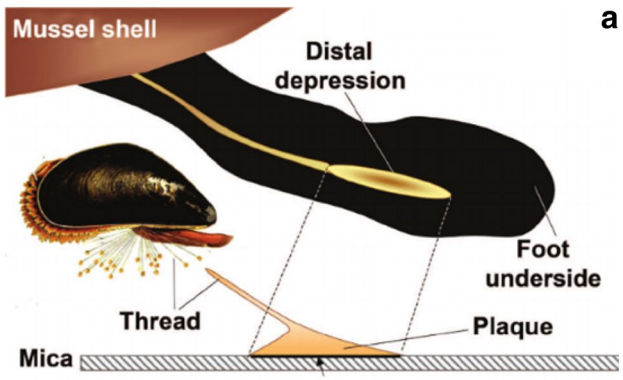

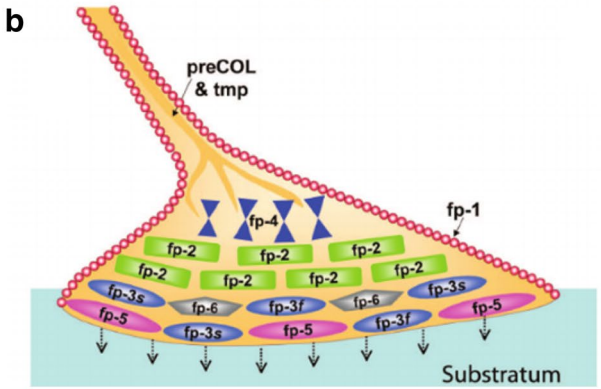

c

Mfp	Dopa %	Lys %	Arg + HyArg %
Mfp-1	15	19.4	1
Mfp-2	5	16.9	9.3
Mfp-3	20	15	9.5
Mfp-5	30	19.5	3.1

Fig. 5 Byssal plaque of the marine mussel. **a** Adhesive plaques are secreted by the mussel foot into the distal depression. This process is repeated to produce a series of radially distributed proteinaceous adhesive plaques and tethers collectively known as the byssus. **b** The relative location of several mussel foot proteins within the adhesive plaque. Mfp-1 is the surface-coating cuticle of the plaque and thread. Mfp-2 is a cohesive structural protein within the plaque. Mfp-3 and Mfp-5 are deposited onto the substratum as a surface-priming layer. **c** Dopa, Lys, and Arg + Arg–OH content of selected Mfps. Figure 5 adapted and developed from [40]

water, and therefore has been extensively utilized in characterization of wet adhesive properties of Mfps [29, 30, 42–45], as well as other compounds, including catechols [46–48]. The geometry of the catechol group is particularly well suited for binding interactions in mica. The hydroxyl spacing on the catechol moiety (~0.29 nm) is commensurate with the spacing of the hydrogen-bond accepting oxygens on the mica surface (0.28 nm) [49, 50]. Several catechol-containing adhesive materials have been compared to their phenol-containing analogs and the switch from the bidentate interaction of catechol to the monodentate interaction of phenol results in a significant decrease in measured adhesion forces [46, 51]. According to Bell theory ($\tau = \tau_0 e^{-E/kT}$), the bidentate hydrogen bonding of catechol to mica ($-E = \sim 28\ kT$) would have a binding lifetime (τ) that is 10^6 times longer than the monodentate form ($-E = \sim 14\ kT$) [50, 52, 53].

The interfacial surface priming adhesive proteins—Mfp-3 and Mfp-5—are relatively low molecular weight, intrinsically unstructured, and adsorb quickly and reversibly to an array of wet surfaces with diverse chemical and physical properties [30]. The participation of Dopa and cationic amino acids in adhesion is supported by AFM results on adhesion properties of Dopa and Lys separately. Atomic force microscopy (AFM) of a single Dopa residue interacting with Titania yields high strength and reversible interactions [54]. This result lent support for Dopa as a key component in the adhesive performance of these surface priming proteins [54]. The prominence of basic residues in Mfp-3 and Mfp-5 enables electrostatic attraction between the positively charged residues within the protein and a range of negatively charged surfaces, including mica and other mineral oxides found in the mussel's intertidal habitat. Adhesive electrostatic interaction between a single Lys residue and a wet mica surface has also been demonstrated with AFM [55]. Increasing solution pH above the Lys amine pKa significantly reduces adhesion and indicates that association of Lys on a wet mica surface requires a cationic amine [55].

SFA adhesion experiments of Mfps on mica surfaces show maximum adhesion at or below pH 3.3. This correlates with the low pH deposition environment in the distal depression of the mussel foot during plaque formation (Fig. 5a) [56]. Measured adhesive forces of Mfps are considerably lower at pH 5.5 and in most cases adhesion is completely abolished above pH 7.5 [29, 40, 43, 52]. pH-dependent oxidation of Dopa has been implicated in the pH dependence of Mfp adhesion [29, 50, 52]. The Dopaquinone product of Dopa oxidation is incapable of hydrogen bond donation, resulting in a loss of adhesion. One notable strategy to prevent Dopa oxidation while enabling surface adhesion is through boronate-complexed Dopa [57]. The Dopa–boronate complex has a weak stability constant and the negative surface charge of mica at pH 7.5 destabilizes and induces dissociation of the borate ion from the complex, leading to Dopa surface binding [57].

Catechol–cation synergy in wet adhesion

While it is not possible to decipher the relative contributions of the adhesive forces of cationic amino acids and Dopa in the Mfps, it is possible to do so in small molecules such as certain siderophores and synthetic analogs. The composition of cyclic trichrysobactin (CTC) resembles

that of adhesive proteins Mfp-3 and Mfp-5 in the proximity and relative ratio of catechol and Lys groups. CTC binds to mica with a significant force of adhesion, F_{ad} of -30 ± 10 mN/m at pH 6.7 [46], compared to Mfp-5 at -65 mN/m measured at pH 2.6 [29] (Note, a negative force of adhesion, by convention denotes an attractive force). The hydration layer thickness (13 ± 1 Å, as measured by the SFA) decreases to 11 ± 1 Å upon the addition of CTC, which is consistent with formation of a CTC monolayer bridging the mica surfaces and displacement of the hydration layer [46].

The tri-serine lactone scaffold of CTC readily hydrolyzes under acidic conditions [7]. Synthetic analogs of CTC in which tris(2-aminoethyl)amine (Tren) replaces the macrolactone core provides a synthetically tractable platform to investigate specific contributions of catechol and Lys to mica adhesion by variation in the amine and aromatic functionalities [46]. Tren-Lys-Cam (TLC) and Tren-Dab-Cam (TDC) (Fig. 6, Group I) retain the catechol and amine, although with variation in the length of the amine side chain. These siderophore analogs replicate strong adhesion to mica observed with CTC. Tren-Lys-Pam (TLP) and Tren-Lys-Bam (TLB) (Fig. 6, Group II) lack catechol but retain Lys. The adhesion energy of TLP and TLB to mica is much weaker than TLC, although the film thickness is small like TLC, presumably because Lys facilitates penetration through the hydration layer on mica. However, the absence of catechol prevents strong adhesion. In Group III analogs (Fig. 6), Tren-Cam(TC) and Tren-Lys^{Ac}-Cam (TL^{Ac}C) retain the catechol group, but reduce the molecular charge of the compound from 4+ to 1+ by acetylation or removal of Lys. Group III siderophore analogs are unable to displace the hydration layer and exhibit no adhesion

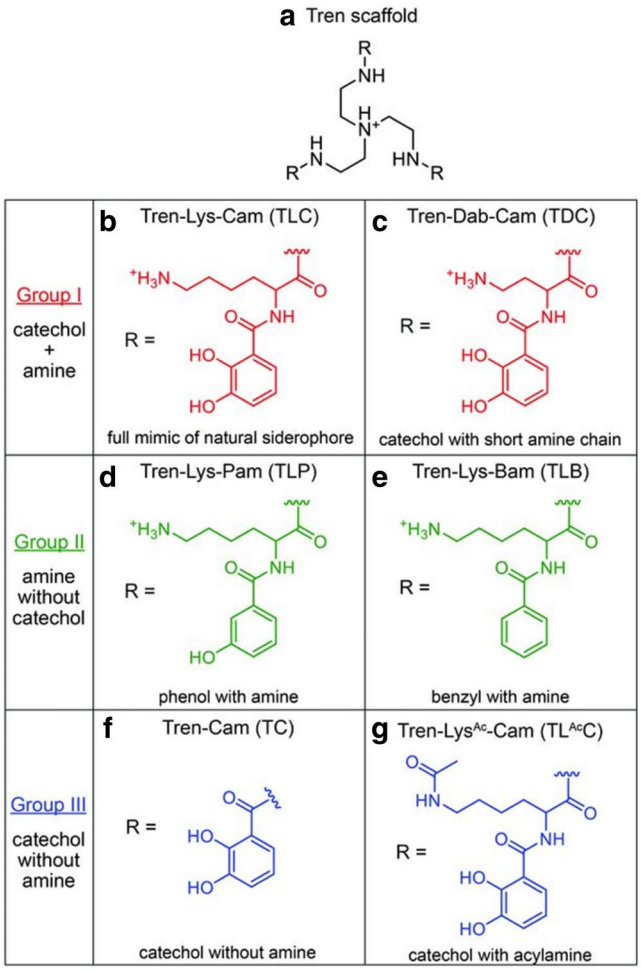

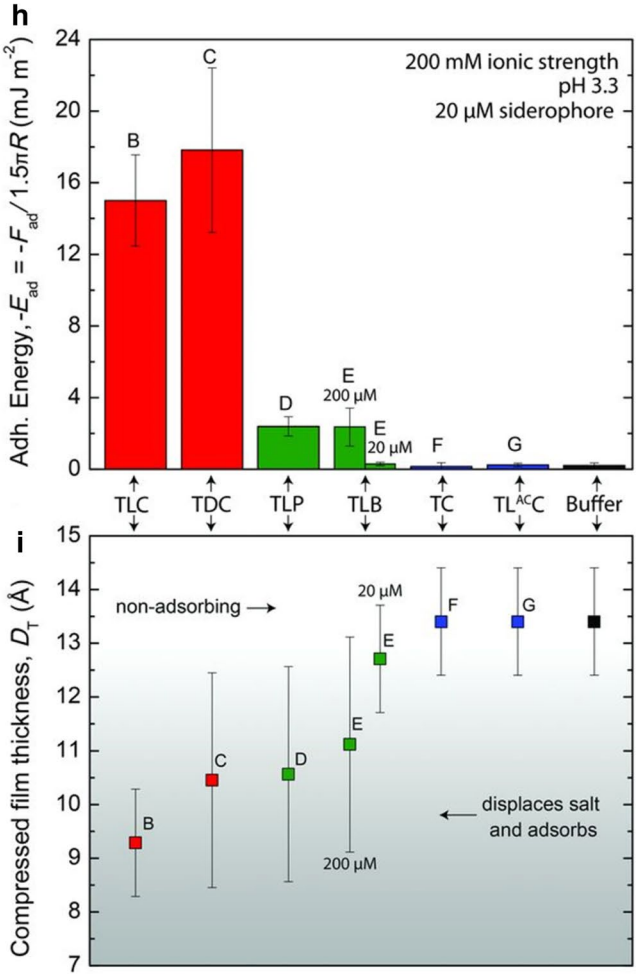

Fig. 6 The synergy of catechol and Lys in siderophore adhesion. **a** Structure of the Tren scaffold. **b**–**g** The R groups appended to Tren. **h** The average adhesion energy required to separate two mica surfaces adsorbed with 1 nmole of the analog (a 20 μM final concentration in the gap solution, except where indicated at 200 μM) in buffer (50 mM acetate + 150 mM KNO_3) at pH 3.3 after 10 min of contact. **i** Thickness of the siderophore monolayer between two mica surfaces at 10mN/m of compressive load. The film thicknesses correspond with the adhesion energy displayed in **h**. A decreased film thickness (<12 Å) indicates that siderophore analogs b, c, d, and e (200 μM) adsorb, displace hydrated salt at the mica surface, and mediate adhesion between two mica surfaces. Figure 6 reproduced from [46]

despite the presence of intact catechol. Only when both catechol and cationic groups are present do these siderophore analogs display strong adhesion. These observations are consistent with a mechanism whereby the cationic primary amine of Lys is able to disrupt the hydration layer on the mica surface (Fig. 7). Catechol adheres to the mica surface through bidentate interactions once the hydration layer has been breached (Fig. 7). Cationic Lys may also contribute to adhesion through electrostatic interactions with the negatively charged mica surface [47].

Two additional siderophore analogs were synthesized to probe the role of cations in wet adhesion [47]. Tren-Arg-Cam (TAC, Fig. 8a) replaces the Lys residue with an Arg and Tren-Lys-Lys-Cam (TLLC, Fig. 8b) doubles the ratio of Lys to catechol. Both TAC and TLLC perform similarly to TLC in SFA experiments. All three siderophore analogs are able to displace the hydration layer, form a monolayer between the mica surfaces, and produce strong adhesion [47]. However, TAC produces only 50–60% of the maximum TLC adhesion and has a critical adsorption concentration (CAC) approximately 10× higher than TLC. The guanidinium cation is bulkier and has a delocalized charge that is presumably less effective than the primary amine of Lys at hydration layer displacement on mica. Similarly, the smaller K^+ cation has a more favorable adsorption-free energy on mica than the larger Cs^+ cation [58]. TLLC has a 2:1 Lys to catechol ratio rather than the 1:1 ratio of TLC. Therefore, TLLC will have a lower catechol density per unit area, which may explain in the observed ~50% reduction in adhesion energy compared to TLC. However, the higher electrostatic charge density of TLLC compared to TLC improves its ability to penetrate the hydration layer and lowers the CAC by an order of magnitude (Fig. 8c).

TLC ($F_{ad} = -101 \pm 10$ mN/m at pH 3.3) [46] outperforms the most adhesive mussel foot protein, Mfp-5 (−65 mN/m at pH 2.6) [29], and the disparity in adhesion force increases with increasing pH. Dopa (Mfp-type catechol) and 2,3-DHBA (siderophore analog-type catechol) both undergo a pH-dependent oxidation with higher pH promoting faster oxidation rates [46]. However, Dopa in Mfps is much more susceptible to oxidation, which is likely a result of both the 3,4-dihydroxy catechol and the electron donating methyl group playing a significant role promoting Dopa oxidation. In CTC and the siderophore analogs, the electron-withdrawing amide in 2,3-DHBA decreases the rate of autoxidation compared to Dopa and improves adhesive performance to mica at high pH [46]. Thus, unlike Mfps, a pH change from 3.3 to 7.5 causes only a slight decrease in the adhesion energy of siderophore analogs [46].

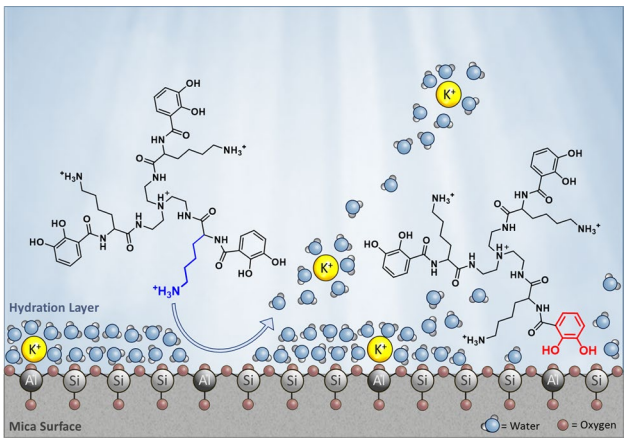

Fig. 7 Catechol-cation synergy in siderophore analogs

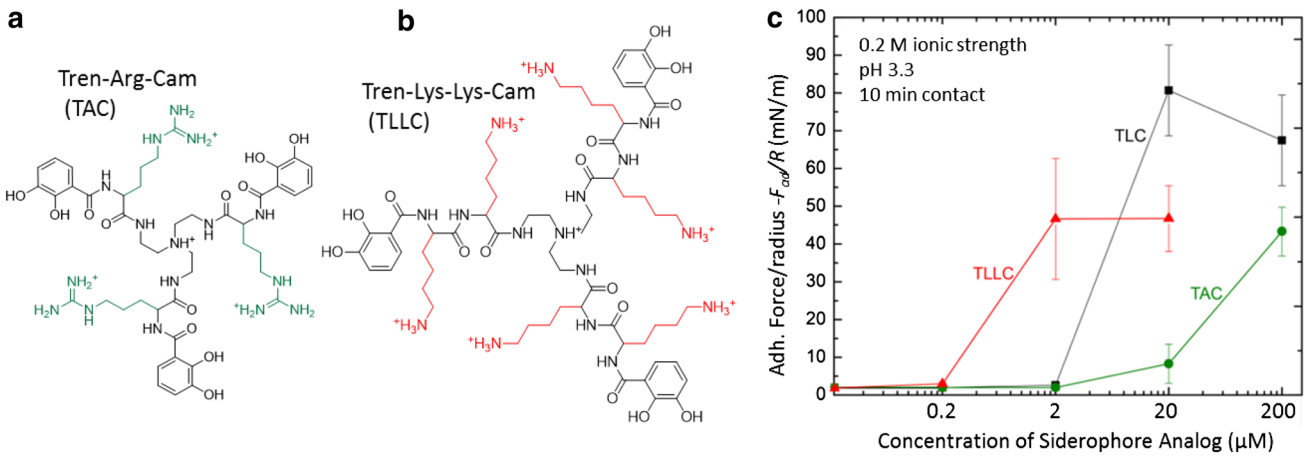

Fig. 8 Critical Adsorption Concentration of TLC, TAC, and TLLC. **a** Structure of Tren-Arg-Cam. **b** Structure of Tren-Lys-Lys-Cam. **c** TLC-, TAC-, and TLLC-mediated adhesion force required to separate two mica surfaces in aqueous solution, as a function of the concentration of the siderophore analogs in the intervening gap solution between the mica surfaces. Figure 8 adapted from [47]

Catechol interactions on titania

Adsorption of catechol [59, 60] and adhesion of single Dopa residues [54] and Dopa-containing Mfp-3 [61] to titania has been extensively studied, in part because of the prevalence of titania in medical implants. Density functional theory studies suggest three distinct adsorption modes of catechol to titania, including bidentate H-bonding, monodentate H-bonding combined with a single coordination bond, and bidentate coordination [59]. These binding modes also likely occur through Dopa in Mfp-3 [61] (Fig. 9), with the balance of the three interaction modes on titania depending largely on the pH [54, 61]. In acidic conditions the protonated form of the Dopa catechol is favored and this leads to the formation of bidentate hydrogen bonding between Dopa hydroxyls and interfacial oxygen atoms on the titania surface. At elevated pH, fully deprotonated Dopa coordinates to the available interfacial Ti^{IV} sites in a bidentate manner [61]. At intermediate pH, a hybrid of these two binding modes is possible.

Bacterial biofilms readily form on titania-coated surgical implants [62]. Attenuated total reflection infrared spectroscopy (ATR-IR) results show that the siderophores, enterobactin and pyoverdine, may play a key role in biofilm initiation on titania [63, 64]. Pyoverdines, produced by many Pseudomonads including *Pseudomonas aeruginosa*, have dihydroxyquinoline and two hydroxamic acid groups that coordinate iron(III). Apo pyoverdines may be bound at the cell surface through the outer membrane FpvA receptor protein [65]. Similarly, apo enterobactin can be bound at the cell surface of *E. coli* through association with the FepA receptor [63]. ATR-IR of free enterobactin and pyoverdine in the presence of Titania surfaces show characteristic absorption bands of catecholate ligands coordinated to metal ions [63, 64]. ATR-IR spectra retain these characteristic features when wild-type *P. aeruginosa* or *E. coli* cells decorated with their respective siderophores are exposed to titania surfaces [63, 64]. A *P. aeruginosa* mutant was produced that lacks the outer membrane pyoverdine receptor, FpvA, and, therefore, cannot bind pyoverdine at the cell surface [64]. The characteristic ATR-IR absorption bands for catechol-titania coordination are absent for the mutant *P. aeruginosa*. These results are consistent with siderophore-initiated bacterial cell attachment to Titania surfaces. Interestingly, catechol can also be used to prevent bacterial attachment to Titania surfaces. Several materials utilize catechol as an anchor for antifouling self-assembled monolayers (SAMs) on Titania as well as other metal oxide [66, 67].

Catechol oxidation

Catechol undergoes pH-dependent oxidation by dioxygen in aqueous solution, producing quinone and hydrogen peroxide [68, 69]. The reactive semiquinone intermediate and quinone product can undergo secondary reactions, forming crosslinked catechol products through aryl coupling, Michael-type addition, Schiff base reaction, and Strecker degradation [70]. The mechanisms of these reactions have been reviewed previously [70].

The reaction sequence of catechol autoxidation is relevant to understanding the formation and function of many biological materials. These materials include Mfps [40, 49, 52], squid beaks [3], sand castle worm cement [4], and melanins [71]. Additionally, antioxidant tea catechins and neurotransmitters (e.g., dopamine, epinephrine, and norepinephrine) are also classes of catechol-containing small molecules that are susceptible to autoxidation [69, 72–74]. Despite the prevalence of catechol autoxidation, many mechanistic details remain to be elucidated.

The autoxidation of catechol has been investigated electrochemically and by tracking dioxygen concentration in aqueous solution [68, 69, 72, 73, 75, 76]. It

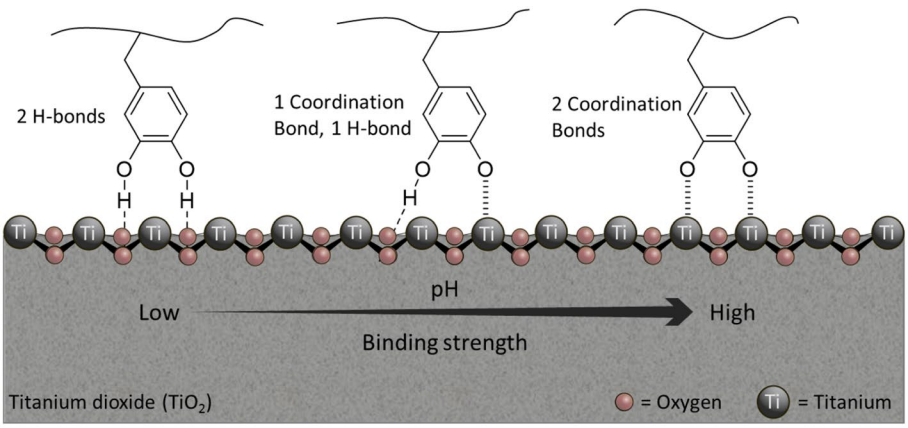

Fig. 9 Binding modes of Dopa to TiO_2. This simplified TiO_2 surface contains titanium atoms (*gray*) and oxygen atoms (*red*). The binding mode of Dopa to TiO_2 is pH dependent with bidentate H-bonding favored below pH 5.5, monodentate H-bonding combined with one coordination bond favored at intermediate pH, and two coordination bonds favored at pH above 7.0. Figure 9 adapted from [61]

is widely accepted that this radical process proceeds through semiquinone and superoxide [69, 72, 76]. However, the lack of agreement on the identity of the initiation reaction of the autoxidation has sparked contrasting interpretations on the mechanism of catechol oxidation by O_2. One interpretation proposes a one-electron oxidation of catechol by dioxygen, involving a direct electron transfer from singlet state catechol to triplet state molecular oxygen [76]. Alternatively, the reaction may begin with the conproportionation of catechol and *o*-quinone to form two equivalents of semiquinone [69]. The more reactive semiquinone can then be oxidized by dioxygen, forming superoxide and quinone. These reactions are summarized in Fig. 10.

The rate of autoxidation of catechol-containing small molecules increases with increasing pH [68, 72, 73, 77–79]. Autoxidation also depends on the nature of the catechol (e.g., 2,3-dihydroxy versus 3,4-dihydroxy catechol), as well as the nature of the substituent groups. A definitive physical organic analysis of aqueous catechol oxidation by dioxygen under physiological relevant conditions is needed to fully understand the natural system and for development of new wet adhesive materials.

Oxidation of catechols by Fe(III) in mussel plaques

Oxidation of catechol, Dopa, and several other 3,4-dihydroxy catechols by Fe(III) occurs in aqueous acidic solution (0.01–1 M H^+) forming quinone and two equivalents of Fe(II) [80–82]. A semiquinone radical intermediate is formed during the rate-determining step, which is subsequently oxidized to quinone by a second equivalent of Fe(III) [81] (Fig. 11).

In addition to Fe(III)–Dopa crosslinking in the mussel plaques described above, Fe(III)-induced oxidation and aryl crosslinking of the 3,4-dihydroxy catechol in Dopa is implicated in the curing process of mussel adhesive plaques [83–86]. Purified Mfp-1 and Mfp-2 precipitate upon addition of Fe(III) at pH 1.5. Analysis of the precipitate reveals the presence of radical species by EPR from high spin Fe(III) and an organic radical [85], presumably Dopa-semiquinone, which readily undergoes aryl coupling [70]. EPR signals are absent in the Fe(III)-free form of Mfp-1 and Mfp-2, suggesting that Dopa-semiquinone appears as a result of Fe(III) addition [85]. Dopa-containing small molecules and model peptides also form covalently crosslinked aryl dimers at pH 2 in the presence of Fe(III) [86]. Fe(III)-dependent dimer formation decreases with increasing pH. Dimerization occurs most readily at pH 2, can be detected at pH 5, and is absent at pH 7 and 9, where Fe(III) coordination is favored over Fe(III) induced oxidation [86]. A Dopa autoxidation product was observed at pH 9 in the absence of Fe(III) and this

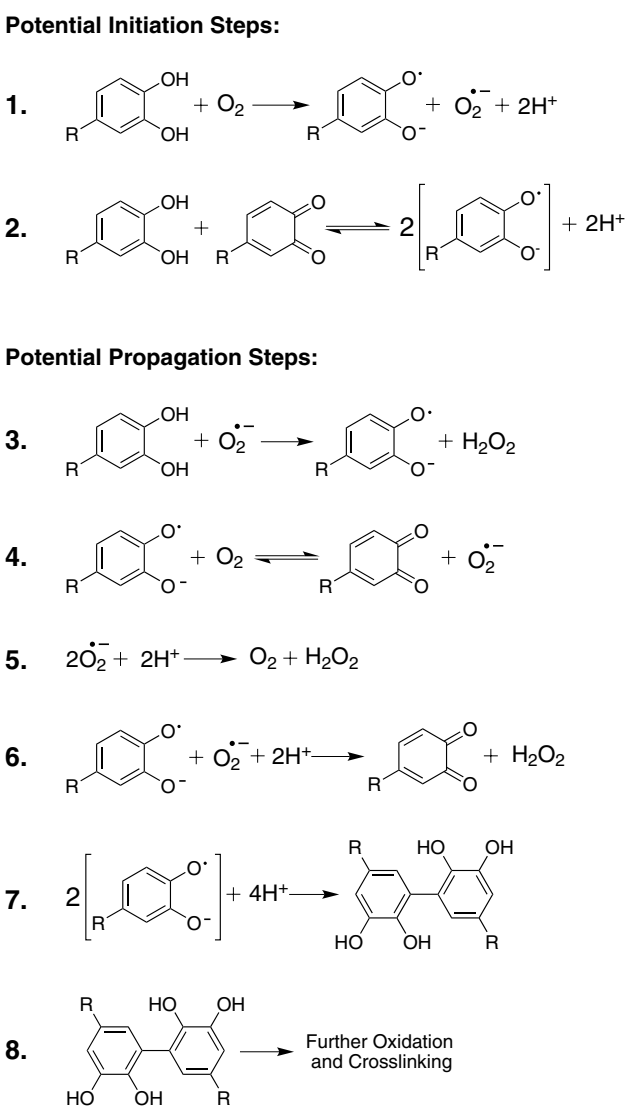

Fig. 10 Potential catechol autoxidation reactions. Catechol autoxidation is initiated either by direct electron transfer from catechol to dioxygen to form semiquinone and superoxide or by the conproportionation of catechol and quinone to form semiquinone. Catechol autoxidation is propagated by steps involving the superoxide or semiquinone radicals. The protonation state of semiquinone is uncertain and reactions shown here involving semiquinone are balanced assuming a deprotonated hydroxyl

product is not detected in the presence of Fe(III), demonstrating that Fe(III) coordination protects Dopa against autoxidation [86].

Collectively, these results imply that a significant number of Fe(III)-induced covalent crosslinks may initially form within the mfps in the plaque in the low pH environment of the distal depression before mussel foot removal allows equilibration to oceanic pH. The pH increase favors Fe(III) coordination to Dopa, which protects the catechol group against oxidation and adds an additional layer of crosslinking in the cured plaque.

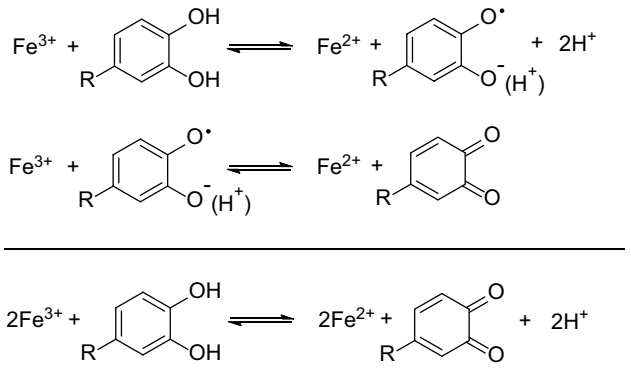

Fig. 11 Redox reactions between iron(III) and catechol in aqueous acidic media. The protonation state of semiquinone is uncertain and reactions shown here involving semiquinone are balanced assuming a deprotonated hydroxyl. Figure 11 adapted from [81]

2,3-DHBA in siderophores and analogs coordinated to Fe(III) in physiological conditions (near neutral pH and higher) is stabilized against catechol oxidation. However, in strongly acidic solution (1 M H^+), Fe(III) catalyzes oxidation of 2,3-DHBA [87]. Thus, 2,3-DHBA behaves similarly to Dopa, although the pH range is shifted, and at physiological pH little if any oxidation of 2,3-DHBA and aryl crosslinking occurs.

Conclusion

The impressive range of catechol chemical reactivity and physicochemical interactions enable its inclusion in a wide range of natural materials, including neurotransmitters, catechins, melanin, bacterial siderophores, and mussel adhesive plaques among others. Fe(III) coordination is especially important in bacterial siderophores—in which catechol binds Fe(III) with exceptionally high affinity. Fe(III) coordination is also essential within mussel adhesive plaques—where Fe(III) coordination to Dopa and Fe(III)-induced oxidation of Dopa lead to Dopa crosslinks that are vital to plaque cohesion. Catechol in siderophore analogs and Mfps is also a key contributor to energetic adhesive interactions on wet surfaces. Cationic residues act in concert with catechol to penetrate interfacial hydration layers that develop on aluminosilicate minerals, including mica and the rocks in the intertidal zone, and adhere to the underlying surface. Parsing catechol interactions in natural adhesive materials aids in the understanding of these complex systems and as a result new synthetic materials are incorporating catechol [42, 85, 88–99] and utilizing its impressive range of chemical reactivity and physicochemical interactions for adhesive and other interactions.

Acknowledgements We are grateful for support from the NSF CHE-1411942 (A.B.) and the NSF Materials Research and Science Engineering Centers Program, DMR-1121053.

References

1. Hickford SJH, Kupper FC, Zhang GP, Carrano CJ, Blunt JW, Butler A (2004) J Nat Prod 67:1897–1899
2. Pfleger BF, Lee JY, Somu RV, Aldrich CC, Hanna PC, Sherman DH (2007) Biochemistry 46:4147–4157
3. Miserez A, Schneberk T, Chengjun S, Frank CW, Waite JH (2008) Science 319:1816–1819
4. Zhao H, Sun C, Stewart RJ, Waite JH (2005) J Biol Chem 280:42938–42944
5. Raymond KN, Dertz EA, Kim SS (2003) Proc Natl Acad Sci U S A 100:3584–3588
6. Reichert J, Sakaitani M, Walsh CT (1992) Protein Sci 1:549–556
7. Sandy M, Butler A (2011) J Nat Prod 74:1207–1212
8. Dertz EA, Xu J, Stintzi A, Raymond KN (2006) J Am Chem Soc 128:22–23
9. Avdeef A, Sofen SR, Bregante TL, Raymond KN (1978) J Am Chem Soc 100:5362–5370
10. Harris WR, Carrano CJ, Cooper SR, Sofen SR, Avdeef AE, McArdle JV, Raymond KN (1979) J Am Chem Soc 101:6097–6104
11. Loomis LD, Raymond KN (1990) Inorg Chem 30:906–911
12. Karpishin TB, Raymond KN (1992) Angew Chem Int Ed Engl 31:466–468
13. Karpishin TB, Dewey TM, Raymond KN (1993) J Am Chem Soc 115:1842–1851
14. Scarrow RC, Ecker DJ, Ng C, Liu S, Raymond KN (1991) Inorg Chem 30:900–906
15. Bluhm ME, Kim SS, Dertz EA, Raymond KN (2002) J Am Chem Soc 124:2436–2437
16. Abergel RJ, Zawadzka AM, Hoette TM, Raymond KN (2009) J Am Chem Soc 131:12682–12692
17. Sandy M, Han A, Blunt J, Munro M, Haygood M, Butler A (2010) J Nat Prod 73:1038–1043
18. Butler A, Theisen RM (2010) Coord Chem Rev 254:288–296
19. Sandy M, Butler A (2009) Chem Rev 109:4580–4595
20. Abergel RJ, Warner JA, Shuh DK, Raymond KN (2006) J Am Chem Soc 128:8920–8931
21. Cohen SM, Raymond KN (2000) Inorg Chem 39:3624–3631
22. Persmark M, Expert D, Neilands JB (1989) J Biol Chem 264:3187–3193
23. Tomisic V, Blanc S, Elhabiri M, Expert D, Albrecht-Gary A-M (2008) Inorg Chem 47:9419–9430
24. Soengas RG, Anta C, Espada A, Paz V, Ares IR, Balado M, Rodríguez J, Lemos ML, Jiménez C (2006) Tetrahedron Lett 47:7113–7116
25. Iglesias E, Brandariz I, Jimenez C, Soengas RG (2011) Metallomics 3:521–528
26. Holten-Andersen N, Harrington MJ, Birkedal H, Lee BP, Messersmith PB, Lee KY, Waite JH (2011) Proc Natl Acad Sci U S A 108:2651–2655
27. Sever MJ, Wilker JJ (2004) Dalton Trans. doi:10.1039/B315811J:1061-1072
28. Menyo MS, Hawker CJ and Waite JH (2013) Soft Matter 9
29. Danner EW, Kan Y, Hammer MU, Israelachvili JN, Waite JH (2012) Biochemistry 51:6511–6518
30. Lu Q, Danner E, Waite JH, Israelachvili JN, Zeng H, Hwang DS (2013) J R Soc Interface 10:20120759

31. Wilker JJ (2010) Angew Chem Int Ed Engl 49:8076–8078
32. Wilker JJ (2010) Curr Opin Chem Biol 14:276–283
33. Harrington MJ, Masic A, Holten-Andersen N, Waite JH, Fratzl P (2010) Science 328:216–220
34. Holten-Andersen N, Mates TE, Toprak MS, Stucky GD, Zok FW, Waite JH (2008) Langmuir 25:3323–3326
35. Hwang DS, Zeng H, Masic A, Harrington MJ, Israelachvili JN, Waite JH (2010) J Biol Chem 285:25850–25858
36. Holten-Andersen N, Fantner GE, Hohlbauch S, Waite JH, Zok FW (2007) Nat Mater 6:669–672
37. Taylor SW, Luther GW III, Waite JH (1994) Inorg Chem 33:5819–5824
38. Werneke SW, Swann C, Farquharson LA, Hamilton KS, Smith AM (2007) J Exp Biol 210:2137–2145
39. Vaccaro E, Waite JH (2001) Biomacromol 2:906–911
40. Nicklisch SC, Waite JH (2012) Biofouling 28:865–877
41. Israelachvili JN, Wennerstrom H (1996) Nature 379:219–225
42. Lee BP, Messersmith PB, Israelachvili JN, Waite JH (2011) Annu Rev Mater Res 41:99–132
43. Wei W, Yu J, Broomell C, Israelachvili JN, Waite JH (2013) J Am Chem Soc 135:377–383
44. Hwang DS, Wei W, Rodriguez-Martinez NR, Danner E, Waite JH (2013) In: Zeng H (ed) Polymer adhesion, friction, a nd lubrication. John Wiley & Sons Inc, Hoboken, NJ
45. Lin Q, Gourdon D, Sun C, Holten-Andersen N, Anderson T, Waite JH, Israelachvili JN (2007) Proc Natl Acad Sci U S A 104:3782–3786
46. Maier GP, Rapp MV, Waite JH, Israelachvili JN, Butler A (2015) Science 349:628–632
47. Rapp MV, Maier GP, Dobbs HA, Higdon NJ, Waite JH, Butler A, Israelachvili JN (2016) J Am Chem Soc 138:9013–9016
48. Ahn BK, Das S, Linstadt R, Kaufman Y, Martinez-Rodriguez NR, Mirshafian R, Kesselman E, Talmon Y, Lipshutz BH, Israelachvili JN, Waite JH (2015) Nat Commun 6:8663
49. Wilker JJ (2011) Nat Chem Biol 7:579–580
50. Yu J, Wei W, Danner E, Ashley RK, Israelachvili JN, Waite JH (2011) Nat Chem Biol 7:588–590
51. Wei W, Yu J, Gebbie MA, Tan Y, Martinez Rodriguez NR, Israelachvili JN, Waite JH (2015) Langmuir 31:1105–1112
52. Yu J, Wei W, Danner E, Israelachvili JN, Waite JH (2011) Adv Mater 23:2362–2366
53. Israelachvili J (2011) Intermolecular and surface forces. Elsevier Inc
54. Lee H, Scherer NF, Messersmith PB (2006) Proc Natl Acad Sci U S A 103:12999–13003
55. Razvag Y, Gutkin V, Reches M (2013) Langmuir 29:10102–10109
56. Martinez Rodriguez NR, Das S, Kaufman Y, Israelachvili JN, Waite JH (2015) Biofouling 31:221–227
57. Kan Y, Danner EW, Israelachvili JN, Chen Y, Waite JH (2014) PLoS ONE 9:e108869
58. Pashley RM (1982) Adv Colloid Interface Sci 16:57–62
59. Terranova U and Bowler DR (2010) j phys Chem C 114:6491-6495
60. Liu Y, Dadap JI, Zimdars D, Eisenthal KB (1999) J Phys Chem B 103:2480–2486
61. Yu J, Wei W, Menyo MS, Masic A, Waite JH, Israelachvili JN (2013) Biomacromol 14:1072–1077
62. Costerton J, Stewart P, Greenberg E (1999) Science 284:1318–1322
63. Upritchard HG, Yang J, Bremer PJ, Lamont IL, McQuillan AJ (2011) Langmuir 27:10587–10596
64. Upritchard HG, Yang J, Bremer PJ, Lamont IL, McQuillan AJ (2007) Langmuir 23:7189–7195
65. Schalk IJ, Hennard C, Dugave C, Poole K, Abdallah MA, Pattus F (2001) Mol Microbiol 39:351–360
66. Lau KH, Ren C, Sileika TS, Park SH, Szleifer I, Messersmith PB (2012) Langmuir 28:16099–16107
67. Kang T, Oh DX, Heo J, Lee HK, Choy S, Hawker CJ, Hwang DS (2015) ACS Appl Mater Interfaces 7:24656–24662
68. Joslyn MA, Branch GEK (1935) J Am Chem Soc 57:1779–1785
69. Li G, Zhang H, Sader F, Vadhavkar N, Njus D (2007) Biochemistry 46:6978–6983
70. Yang J, Cohen Stuart MA, Kamperman M (2014) Chem Soc Rev 43:8271–8298
71. Felix CC, Sealy RC (1981) J Photochem Photobiol 34:423–429
72. Mochizuki M, Yamazaki S, Kano K, Ikeda T (2002) Biochim Biophys Acta 1569:35–44
73. Roginsky V, Alegria AE (2005) J Agric Food Chem 53:4529–4535
74. Roginsky V, Barsukova TK, Bruchelt G, Stegmann HB (1997) Z Naturforsch 53:380–390
75. Nematollahi D, Taherpour A, Jameh-Bozorghi S, Mansouri A, Dadpou B (2010) Int J Electrochem Sci 5:867–879
76. Shendrik AN, Odaryuk ID, Kanibolotska LV, Kalinichenko EA, Tsyapalo AS, Beznos VV, Kanibolotsky AL (2012) Int J Chem Kinet 44:414–422
77. Heacock RA (1959) Chem Rev 59:181–237
78. Bors W, Saran M, Michel C, Lengfelder E, Fuchs C, Spottl R (1975) Int J Radiat Biol Relat Stud Phys Chem Med 28:353–371
79. Bors W, Michel C, Manfred S, Lengfelder E (1978) Biochim Biophys Acta 540:162–172
80. Mentasti E and Pelizzetti E (1973) J Chem Soc Dalton Trans:2605
81. Mentasti E, Pelizzetti E and Saini G (1973) J Chem Soc Dalton Trans:2609-2614
82. Mentasti E, Pelizzetti E, Baiocchi C (1976) J Inorg Nucl Chem 38:2017–2021
83. Burzio LA, Waite JH (2000) Biochemistry 39:11147–11153
84. Miaoer Y, Hwang JW, Deming TJ (1999) J Am Chem Soc 121:5825–5826
85. Sever MJ, Weisser JT, Monahan J, Srinivasan S, Wilker JJ (2004) Angew Chem Int Ed Engl 43:448–450
86. Fullenkamp DE, Barrett DG, Miller DR, Kurutz JW, Messersmith PB (2014) RSC Adv 4:25127–25134
87. Xu J, Jordan RB (1988) Inorg Chem 27:4563–4566
88. Matos-Perez CR, Wilker JJ (2012) Macromolecules 45:6634–6639
89. Matos-Perez CR, White JD, Wilker JJ (2012) J Am Chem Soc 134:9498–9505
90. Lee H, Dellatore SM, Miller WM, Messersmith PB (2007) Science 318:426–430
91. Kim BJ, Oh DX, Kim S, Seo JH, Hwang DS, Masic A, Han DK, Cha HJ (2014) Biomacromol 15:1579–1585
92. Cencer M, Murley M, Liu Y, Lee BP (2015) Biomacromol 16:404–410
93. Cencer M, Liu Y, Winter A, Murley M, Meng H, Lee BP (2014) Biomacromol 15:2861–2869
94. Barrett DG, Bushnell GG, Messersmith PB (2013) Adv Healthc Mater 2:745–755
95. Lee J, Yang SH, Hong SP, Hong D, Lee H, Lee HY, Kim YG, Choi IS (2013) Macromol Rapid Commun 34:1351–1356
96. Yang SH, Kang SM, Lee KB, Chung TD, Lee H, Choi IS (2011) J Am Chem Soc 133:2795–2797
97. Sedo J, Saiz-Poseu J, Busque F, Ruiz-Molina D (2013) Adv Mater 25:653–701
98. White JD, Wilker JJ (2011) Macromolecules 44:5085–5088
99. Brubaker CE, Kissler H, Wang LJ, Kaufman DB, Messersmith PB (2010) Biomaterials 31:420–427